AGU PUBLICATIONS

JGR

Journal of Geophysical Research: Oceans

RESEARCH ARTICLE

10.1002/2016JC011646

Key Points:
- The MAB winter/spring temperature is largely determined by the initial temperature and mean cumulative air-sea flux
- Air-sea and ocean advective flux contributions to temperature anomaly vary from year to year
- The predictability of spring temperature anomaly is tractable within a 2 month time scale

Correspondence to:
K. Chen,
kchen@whoi.edu

Citation:
Chen, K., Y.-O. Kwon, and G. Gawarkiewicz (2016), Interannual variability of winter-spring temperature in the Middle Atlantic Bight: Relative contributions of atmospheric and oceanic processes, *J. Geophys. Res. Oceans*, *121*, 4209–4227, doi:10.1002/2016JC011646.

Received 13 JAN 2016
Accepted 16 MAY 2016
Accepted article online 13 JUN 2016
Published online 18 JUN 2016

© 2016. American Geophysical Union. All Rights Reserved.

Interannual variability of winter-spring temperature in the Middle Atlantic Bight: Relative contributions of atmospheric and oceanic processes

Ke Chen[1], Young-Oh Kwon[1], and Glen Gawarkiewicz[1]

[1]Physical Oceanography Department, Woods Hole Oceanographic Institution, Woods Hole, Massachusetts, USA

Abstract Relative contributions between the local atmospheric and oceanic processes on the interannual variability of winter-spring shelf temperature in the Middle Atlantic Bight (MAB) are investigated based on a regional ocean model. The model demonstrates sufficient capability to realistically simulate the interannual temperature changes during 2003–2014. On interannual time scales, the mean winter/spring temperature in the MAB is determined by the combination of the initial temperature at the beginning of the season and the mean cumulative air-sea flux, while the mean cumulative ocean advective flux plays a secondary role. In spite of the overall importance of air-sea flux in determining the winter and spring temperature, the relative contributions between air-sea flux and ocean advective flux on the evolution of the temperature anomaly in each individual year varies. The predictability of spring (April–June) temperature based on winter (January–March) temperature is weak because the temporal decorrelation time scale changes significantly from year to year. Both the highly variable shelf temperature and its decorrelation time scale are affected by the changes in the relative contributions between the air-sea flux and ocean advective flux.

1. Introduction

The Middle Atlantic Bight continental shelf (MAB, Figure 1) off the northeastern U.S. is a dynamic and highly productive system supporting economically important commercial fisheries. There is growing evidence that climate changes impact the MAB physical environment [e.g., *Shearman and Lentz*, 2010] and hence the ecosystem, including the stocks and spatial distribution of commercially important fish and benthic invertebrates [e.g., *Nye et al.*, 2009; *Lucey and Nye*, 2010; *Walsh et al.*, 2015]. Understanding of the processes controlling the coastal physical environment, e.g., the temperature variability within the context of climate change is thus fundamentally important.

The ocean temperature in this region experienced an extreme warming event in 2012, which greatly impacted the coastal ecosystem and commercial fisheries [*Friedland*, 2012; *Gawarkiewicz et al.*, 2013; *Mills et al.*, 2013]. The extreme temperature anomaly resulted in a northward shift in the distribution of Atlantic cod in this region [*Friedland*, 2012], increased abundance of squid in the summer of 2012, and introduced warm water species not previously seen off southern New England [*Gawarkiewicz et al.*, 2013]. Such an extreme event in the MAB was attributed to the anomalous atmospheric forcing, which was linked to the northward shift in the jet stream position [*Chen et al.*, 2014a, 2015]. The anomalously warm atmospheric conditions in the winter of 2011–2012 increased the ocean heat content (increased the ocean heat content anomaly) and facilitated the extreme warm ocean temperature in spring 2012 [*Chen et al.*, 2014a, 2015]. On the other hand, the ocean advection played a secondary role, which partially damped the heat content anomaly created by the air-sea heat flux [*Chen et al.*, 2015].

While the atmospheric forcing was the major driver of the 2012 extreme warming over intraseasonal to seasonal time scales, the relative importance of atmospheric forcing versus ocean advection over interannual and longer time scales has yet to be clarified. Prior studies have arrived at different conclusions, likely due to the different seasons, years, and time scales considered in each study. For example, *Thompson et al.* [1988] showed that the spatial patterns associated with interannual variability of sea surface temperature (SST) are consistent with the changes in the onshore (offshore) geostrophic winds that advect warm and

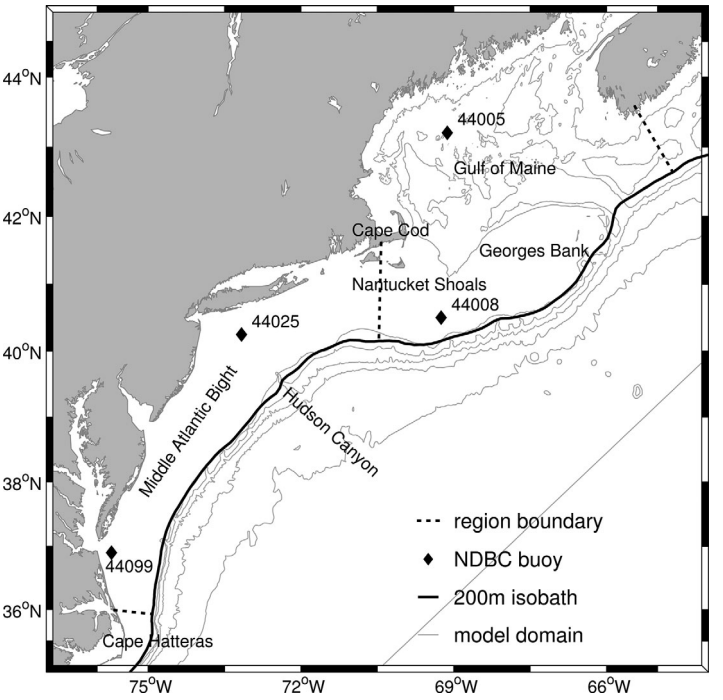

Figure 1. Map showing the Middle Atlantic Bight (MAB) and Gulf of Maine (GoM) region. Locations of four NDBC buoys are labeled in diamond. The smoothed 200 m isobath (black curve) and black dashed lines define the boundaries of the region of the GoM and MAB. The 100, 200, 1000, 2000, and 3000 m isobaths are contoured in gray. The gray straight line denotes the offshore boundary of the model.

moist (cold and dry) air over the ocean. *Mountain* [2003] suggested that decadal variability of the MAB shelf temperature was largely due to changes in local atmospheric heat flux. However, *Shearman and Lentz* [2010] demonstrated that the long-term interannual SST change in the MAB is best explained by changes in the along-shelf ocean advection from the Labrador Sea. A more recent analysis indicated that the interannual change of shelf temperature off the New Jersey coast is more likely related to cross-shelf shifts of the shelf break front [*Forsyth et al*., 2015]. Therefore, elucidating the relative contributions of oceanic processes versus atmospheric processes in determining the interannual variability of the shelf temperature requires further investigation.

Better understanding of year-to-year variability of ocean temperature in this region, especially extremes such as the 2012 warming, would help provide the scientific basis necessary for improving ecosystem management and thus has important economic impacts for the commercial fishing industry. This is also critical considering the increasing frequency of extreme events in the climate system [*Rahmstorf and Coumou*, 2011; *Coumou and Rahmstorf*, 2012; *Hansen et al*., 2012]. For example, most of North America experienced record-breaking low air temperatures in January 2014, only 2 years after the extremely warm winter in 2011–2012.

In this work, we extend the case study of the 2012 extreme warming event to multiple years during the winter and spring. As stated in earlier studies [e.g., *Lentz*, 2010; *Chen et al*., 2015], the limited subsurface observations make it difficult to accurately quantify the heat balance in the MAB, particularly over interannual and longer time scales. Therefore, we employ numerical modeling to investigate the interannual variability of winter-spring temperature in the MAB, specifically to address the following scientific questions. What is the response of the shelf temperature in the MAB to extreme year-to-year variability of the atmospheric and offshore oceanographic forcing? To what extent is the interannual variability of temperature in the MAB, especially the extreme events, due to the atmospheric forcing as suggested from the winter 2011–2012? How does the relative importance of ocean advection versus atmospheric forcing change from year to year? The analysis will focus on the winter (January-February-March, JFM) and spring (April-May-June, AMJ) period, when interannual anomalies are the largest [*Joyce*, 2002; *Connolly and Lentz*, 2014]. This is also the seasonal time frame when the extreme warm anomaly in 2012 and the record-low temperatures in early 2014 occurred. Winter-spring ocean temperature also largely controls the winter-spring phytoplankton bloom [e.g., *Miller*, 2004], and has important implications for the formation and decay of the MAB cold pool [e.g., *Ketchum and Corwin*, 1964; *Houghton et al*., 1982].

In the following, we provide a brief description of the model configuration, the forcing, data used for the verification of the model, and the performance of the model in section 2. The interannual variability of winter-spring temperature in the MAB associated with the atmospheric and oceanic processes is described in section 3. Section 4 discusses the interannually varying decorrelation time scale and implications for the predictability of MAB shelf temperature during winter and spring. The linkage of the shelf thermal

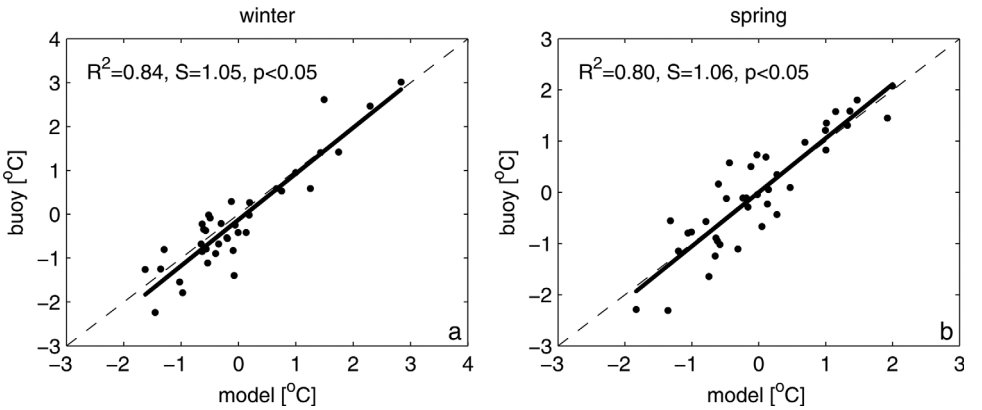

Figure 2. Comparison of (a) winter (January–March) and (b) spring (April–June) SST anomalies from the model and buoys (NDBC 44005, 44008, 44025, 44099) during 2003–2014. R-squared values (R^2) and regression slopes (S) are shown.

environment to large-scale atmospheric and oceanic processes is discussed in section 5 followed by a summary in section 6.

2. Model and Data

2.1. Numerical Model

The modeling strategy follows *Chen et al*. [2015]. Here we review some of the model configurations particularly relevant to this study. More detailed information can be found in earlier studies [*Chen et al*., 2014b, 2015; *Chen and He*, 2015].

The model utilized in this study is a shelf-wide ocean circulation model, based on the hydrostatic Regional Ocean Modeling System (ROMS). ROMS is a free-surface, primitive equation model in widespread use for estuarine, coastal, and basin-scale ocean applications (www.myroms.org/papers). ROMS employs split-explicit separation of fast barotropic and slow baroclinic modes, and is formulated in vertically stretched terrain following coordinates using algorithms described in detail by *Shchepetkin and McWilliams* [2005] and *Haidvogel et al*. [2008]. A redefinition of the barotropic pressure-gradient term [*Shchepetkin and McWilliams*, 2005] is also applied in ROMS to reduce the pressure-gradient truncation error. Our regional model domain encompasses both the MAB and Gulf of Maine (GoM) (hereinafter, MABGOM model), bounded by Cape Hatteras in the southwest and Nova Scotia in the northeast [*Chen et al*., 2015, Figure 2]. The model's horizontal resolution is 10 km in the along-shelf direction, and 6 km in the cross-shelf direction. Vertically, there are 36 terrain-following levels in the water column with higher resolution near the surface and bottom in order to better resolve ocean boundary layers. A generic-length scale (GLS) turbulent mixing closure k-kl scheme [*Warner et al*., 2005] was used to calculate vertical mixing and bottom stress was computed using a quadratic method with a drag coefficient of 0.003.

For the surface forcing of the model, we employ a scheme that combines air-sea flux calculated using bulk formulae and a surface thermal correction based on high-resolution SST maps. This scheme has been applied previously to provide realistic forcing of air-sea exchange [*Chen and He*, 2010]. The bulk formulae calculation [*Fairall et al*., 2003] is based on three hourly and ~18 km resolution meteorological data (surface winds, air temperature, air pressure, relative humidity, short wave radiation, long wave radiation, cloud coverage, and precipitation) from the National Center for Environment Prediction (NCEP) North America Regional Reanalysis (NARR). This calculation provides large-scale variability in the fluxes of momentum and buoyancy at the ocean surface, but is incapable of reproducing some fine-scale structures due to low spatial resolution of the meteorological data. To compensate for this deficiency in the surface forcing, the surface thermal correction adjusts the surface heat flux based on the difference of the model SST and multiplatform blended SST from National Oceanic and Atmospheric Administration (NOAA) OceanWatch. The adjustment time scale is 3 h, consistent with the temporal resolution of the NARR product. Additional sensitivity experiments using a relaxation coefficient based on bulk flux formulas [*Barnier et al*., 1995] and no adjustment of surface forcing indicate that the major results discussed in sections 3 and 4 are insensitive to this choice (see the Appendix A).

Freshwater runoff from nine major rivers in the region was also imposed. These include the St. John, Penobscot, Kennebec, Androscoggin, Merrimack, Connecticut, Hudson, Delaware, and Potomac Rivers. For each river, United State Geological Survey (USGS) real-time runoff measurements were used to specify freshwater volume transport and temperature.

The model initial and boundary conditions are extracted from a product that combines the mesoscale variability from a data-assimilative global ocean circulation model, Hybrid Coordinate Ocean Model [*Chassignet et al*., 2006] plus Navy Coupled Ocean Data Assimilation (HYCOM/NCODA), with the background mean fields from the temperature and salinity climatology of the World Ocean Atlas (WOA) 2013. The HYCOM/NCODA data set (publicly available at: https://hycom.org) provides daily prognostic ocean state variables on a 1/12° horizontal grid with 33 depth levels. Due to the missing dynamics (e.g., river inflow) of global models in the coastal region, the HYCOM/NCODA data set has a systematic temperature and salinity bias, particularly on the continental shelf. We corrected the HYCOM/NCODA data against the temperature and salinity climatology from the World Ocean Atlas (WOA) 2013 (version 2). Removing the mean bias is especially important in this study in which we aim to investigate the temperature variability on the shelf. This correction is particularly important considering the long-term warming trend in the Northeast coastal ocean [*Chen et al*., 2015]. In the correction, the climatological monthly means of temperature and salinity from the HYCOM/NCODA data set were replaced by climatological monthly means from the WOA, while the variability, i.e., the deviations from the climatological mean, was retained. Similarly, the mean dynamic height and associated geostrophic transport were computed along the southwestern and northeastern boundaries based on the WOA monthly mean temperature and salinity. Then the monthly mean dynamic height and geostrophic transport from HYCOM/NCODA were corrected by their counterparts from the WOA climatology. In doing so, we remove the mean biases in the hydrography used for the boundary condition in a dynamically consistent way.

Temperature and salinity in the open ocean (with the bottom depth deeper than 2000 m) in the MABGOM model were nudged back to the corrected, four-dimensional temperature/salinity field from HYCOM/NCODA. The nudging time scale is 2 days at the open boundary and increases linearly to a very long time scale (1000 days) at the 2000 m isobath, which results in nudging strength decreasing gradually from the open boundary toward the interior. No nudging was applied in regions of water depth shallower than 2000 m. Generally, the data-assimilative HYCOM/NCODA provides good estimates of the mesoscale variability in the open ocean, particularly on the formation of Gulf Stream meanders and the location and intensity of warm core rings in the slope sea. With the temperature and salinity nudging in the Gulf Stream/Slope Sea region, the model is able to realistically capture the meandering of the Gulf Stream and the hydrography in the Slope region and is able to provide vital information for estimating the cross-shelf heat flux. The 2000 m isobath generally follows the orientation of the shelf break (∼200 m isobath), and the distance between the shelf break and 2000 m isobath varies from 50 to 70 km, larger than the characteristic spatial scales (10–30 km) in this region [*Todd et al*., 2012]. Therefore, the nudging only constrains conditions in the open ocean and allows dynamical processes to evolve freely exchanging water masses between the open ocean and the shelf.

Subtidal free-surface and 2-D momentum boundary conditions of the MABGOM model were derived from the corrected HYCOM/NCODA fields using an explicit Chapman [*Chapman*, 1985] and Shchepetkin scheme [*Mason et al*., 2010], plus M2 tidal harmonics from an Advanced Circulation Model for Oceanic, Coastal and Estuarine Waters (ADCIRC) tidal simulation of the western Atlantic [*Luettich et al*., 1992]. An Orlanski-type radiation [*Orlanski*, 1976] boundary condition was used for 3-D state variables.

Focusing on the winter-spring temperature, we conducted hindcast simulations from 1 December to 30 June of each year from 2003 to 2014. This strategy reduces the computation load relative to a continuous forward run through the entire time period 2003–2014. The model initializes each year on 1 December, and runs through the end of June of the following year. So for each year, the initial condition is directly from the data-assimilative HYCOM/NCODA, yielding more realistic initial conditions for each year.

2.2. Data

We use satellite-based SST data for surface thermal correction (see section 2.1). The SST product developed by the NOAA OceanWatch is a blended product of SST observations from both microwave and infrared sensors carried on multiple platforms including GOES, AVHRR, and MODIS satellites. This product is available every day from July 2002 to the present with a horizontal resolution of ∼10 km (0.1°). Near-surface temperature data from four National Data Buoy Center (NDBC) buoys within the MAB and GoM (see Figure 1 for the

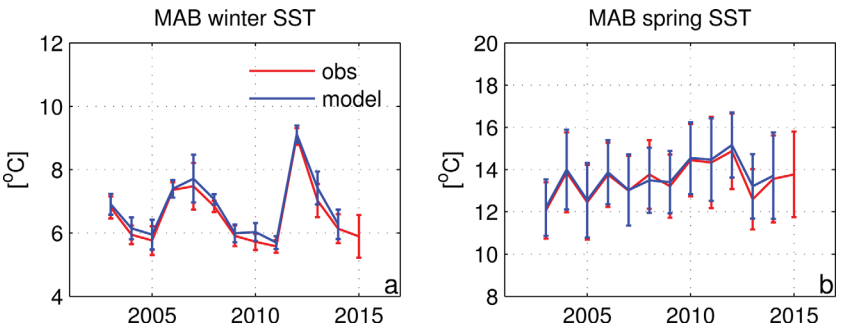

Figure 3. Mean SST of MAB in (a) winter and (b) spring. NOAA blended SST and model SST during 2003–2014 are shown in red and blue, respectively. Error bars represent standard error during temporal averaging. Degrees of freedom in calculating the standard error is based on the integration of autocorrelation considering serial correlation [*Emery and Thomson*, 2001].

locations) are used to compare against the model simulation. These buoys are located in the GoM (44005), on the continental shelf near Nantucket (44008), south of Long Island (44025), and offshore of Virginia Beach (44099).

2.3. Model-Data Comparison

Extensive model/observation comparisons in previous studies using similar model configurations indicate that the MABGOM model is able to successfully reproduce the temporal and spatial variability of the regional circulation during 2004–2013 [*Chen et al.*, 2015; *Chen and He*, 2015]. For the purpose of this study, we further validate the model skill against available observations over interannual time scales.

We first compare the seasonal mean temperature anomaly in winter and spring between the model and four NDBC buoys. The water temperature recorded at the buoy represents the temperature in the upper couple of meters as opposed to skin temperature. This is comparable to the temperature in the top layer of the model. As shown in Figure 2, our model hindcast accurately captures the interannual variability of the near-surface temperature. For both winter and spring, the R-squared value is no less than 0.8, and the regression slope is close to 1. Also, the Pearson correlation between temperature anomalies from the model and buoy for each period is significant at the 95% confidence level.

We next compare the modeled MAB winter and spring mean SST against blended SST data from NOAA OceanWatch (Figure 3). The mean winter SST in the MAB ranges from 5.6 to 9°C during 2003–2014. The model successfully captures the interannual variability of winter temperature. The model-data difference is small (<0.4°C), well within the standard error of the observed data. For spring, the seasonal mean temperature varies from 12 to 14.9°C from year to year. In comparison, winter mean SST has larger interannual variability, consistent with earlier studies [*Joyce*, 2002; *Connolly and Lentz*, 2014]. Again, the model hindcast compares well with the observations.

3. Interannual Winter-Spring Temperature Budget

Neglecting horizontal diffusion, the seasonal mean, depth-averaged temperature $\overline{T}$ is determined by the initial temperature at the beginning of the season T_o, the mean cumulative air-sea flux $\overline{T_{air}}$, and mean cumulative ocean advective flux $\overline{T_{adv}}$:

$$\overline{T} = T_o + \overline{T_{air}} + \overline{T_{adv}} \tag{1}$$

where $\overline{T} = \frac{\int_{t_1}^{t_2} T dt}{t_2 - t_1}$, $\overline{T_{air}} = \frac{\int_{t_1}^{t_2} T_{air} dt}{t_2 - t_1}$, $\overline{T_{adv}} = \frac{\int_{t_1}^{t_2} T_{adv} dt}{t_2 - t_1}$,

$$T_{air} = \int_{t_1}^{t} Q_{air} dt' = \int_{t_1}^{t} \frac{Q}{\rho_o c_p H} dt', \; T_{adv} = \int_{t_1}^{t} Q_{adv} dt' = \int_{t_1}^{t} \left(-\frac{1}{H} \int_{-H}^{0} \nabla(\mathbf{u}T) dz \right) dt',$$

where t is time during winter-spring, t_1 and t_2 are the starting and ending time of each winter/spring, T is the depth-averaged temperature at time t, Q is the net air-sea flux (positive downward) at time t, ρ_o is the

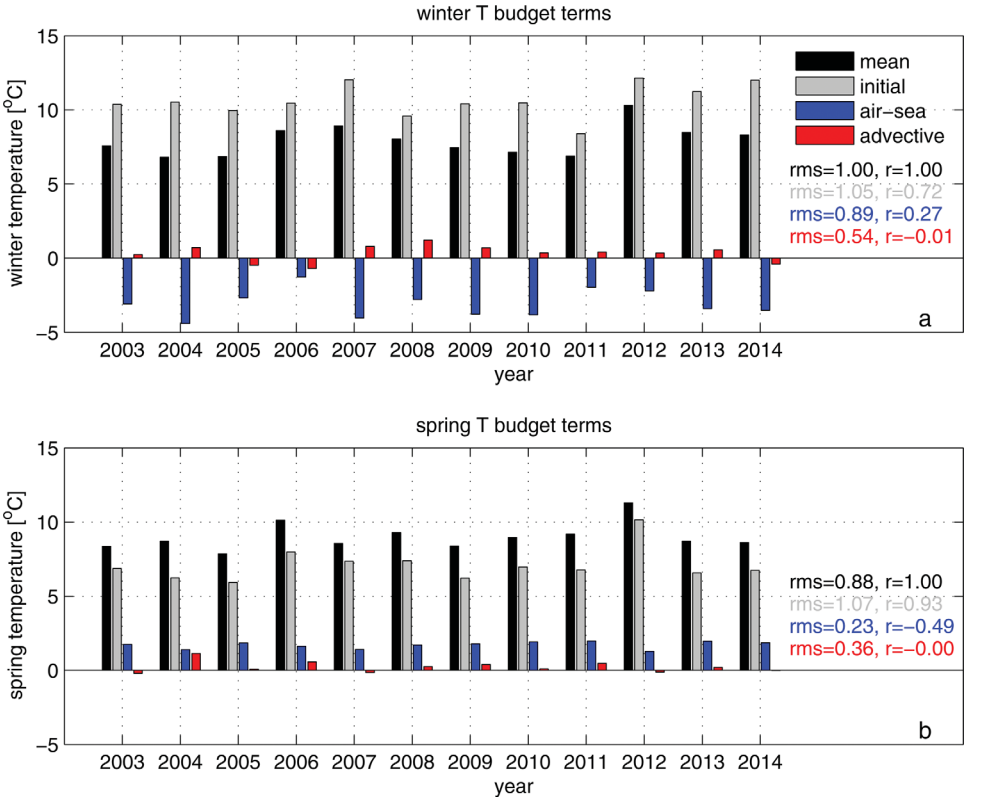

Figure 4. (a) Winter and (b) spring temperature budget terms for each year from equation (2). The seasonal mean temperature, initial temperature, mean cumulative air-sea, and ocean advective flux are shown in black, gray, blue, and red. Corresponding root-mean-square (RMS) and correlation (r) values are also shown.

average seawater density (1024 kg m^{-3}), c_p is the specific heat capacity of seawater (3985 J kg^{-1} $°C^{-1}$), H is the water column thickness, and **u** is the horizontal velocity vector. Notice that Q_{air} is denoted as the air-sea flux with a unit of °C s^{-1}, and T_{air} is denoted as the cumulative air-sea flux with a unit of °C. For this study, we focus on the temperature variability over the entire MAB shelf. Considering the control volume of the MAB (Figure 1), the volume-averaged seasonal mean temperature is:

$$\widetilde{\overline{T}} = \widetilde{T_o} + \widetilde{\overline{T_{air}}} + \widetilde{\overline{T_{adv}}} \tag{2}$$

where the tilde represents volume-averaging over depth-averaged terms, which is

$$\tilde{()} = \frac{\iint ()H(x,y,t)\cdot s(x,y)dxdy}{\iint H(x,y,t)\cdot s(x,y)dxdy}$$

and the time-evolving water column thickness H and spatially varying grid area s are considered. For the ease of presentation, we neglect the tildes in (2) in the following discussions. So $\overline{T}$, T_o, $\overline{T_{air}}$, and $\overline{T_{adv}}$ are referred to as the volume-averaged quantities. For the heat balance of the control volume of the MAB, the volume-averaged advective flux is equivalent to flux convergence across the boundaries of the control volume: the 200 m isobath and two cross-shelf sections at the north and sound end of the MAB (Figure 1).

Based on the model hindcast, the budget terms for mean winter (JFM) and spring (AMJ) temperature during 2003–2014 are calculated (Figure 4). The mean winter temperature in the MAB has notable interannual variability, with a root-mean-square (RMS) value of 1.00°C. All winters show consistent cooling which is the result of air-sea flux. In comparison, the ocean advective flux has both warming and cooling effects depending on the year, with a much smaller RMS compared to that of air-sea flux or mean temperature. The mean spring temperature has a smaller interannual variability, with a RMS of 0.88°C. The consistent warming during this time of the year is again controlled by the air-sea flux, which constitutes the seasonal warming.

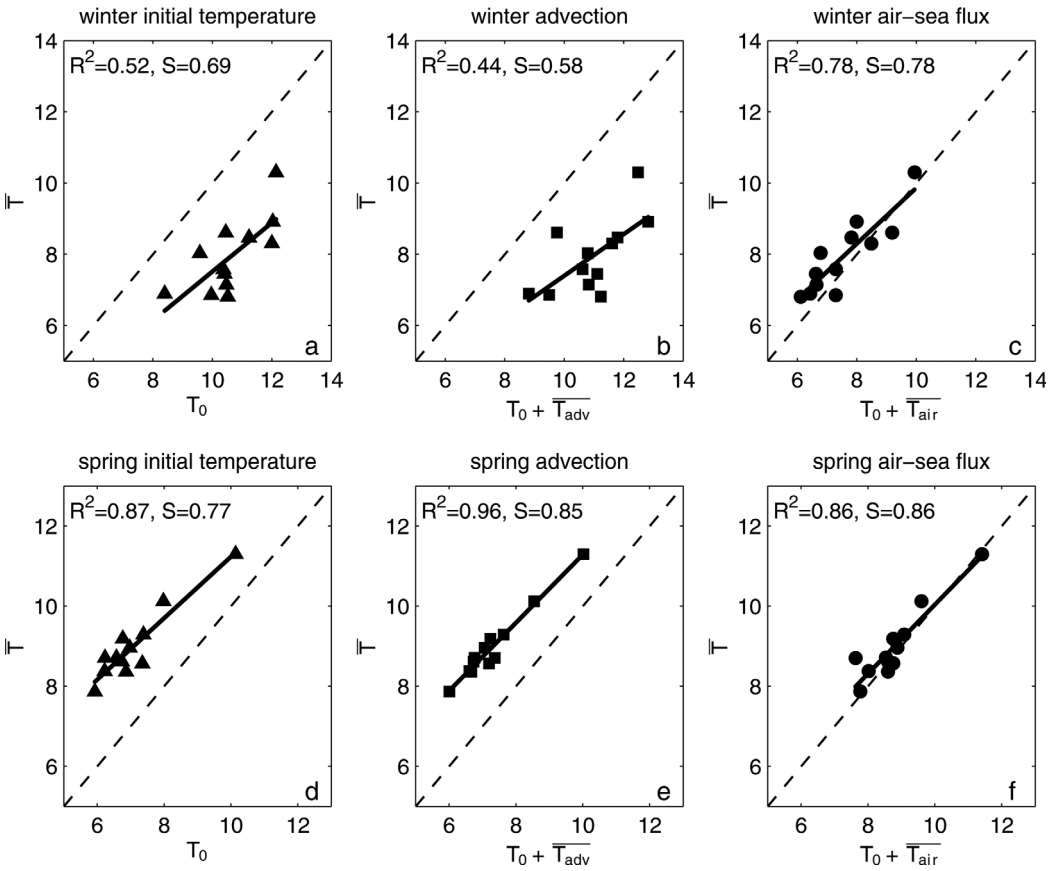

Figure 5. The relationship between winter and spring temperatures and different terms as defined in equation (2). (a and d) Initial temperature, (b and e) initial temperature and mean cumulative ocean advective flux, and (c and f) initial temperature and mean cumulative air-sea flux (unit: °C). R-squared (R^2) and regression slopes (S) are shown.

Ocean advective flux, which has a larger RMS value than that of the air-sea flux, plays variable roles in controlling the spring mean temperature from year to year.

For both winter and spring, the initial temperature is the most dominant factor in determining the interannual variability of the seasonal mean temperature. For example, the extreme warm winter and spring in 2012 are both accompanied by the warmest initial temperatures at the beginning of the season in the 12 years examined here. In addition to the warmest initial temperatures, the earlier analysis also showed that the slower cooling rate during fall and winter of 2011–2012 contributed to the record-high temperature in spring 2012 [*Chen et al.*, 2014a]. The degree to which both the cumulative air-sea and ocean advective flux act on changing the initial temperature determines the mean winter/spring temperature. Nevertheless, T_o exhibits the best interannual correlation by far with the seasonal mean temperature in both winter ($r = 0.72$) and spring ($r = 0.93$) (Figure 4).

The relative roles of T_o, $\overline{T_{adv}}$, and $\overline{T_{air}}$ (volume-averaged quantities) in determining the winter and spring temperature, respectively, from year to year are further quantified (Figure 5). We use the three different types of information from the linear regression analysis, i.e., R-squared (R^2) value, regression slope (S), and proximity to the one-to-one line, to describe the relative importance of each term for determining each season's mean temperature. The R^2 value indicates how linearly the interannual variations of two variables are related. However, the R^2 value does not provide any information about the relative amplitude between the interannual variability of two variables, and thus we also need to consider S. The S being less than one indicates larger variability of the explanatory variable, and S close to one indicates comparable variability of the explanatory and dependent variables. Furthermore, the S and R^2 do not contain information about the comparability between the absolute amplitudes of the two variables, which is reflected in the overall proximity of the data points to the one-to-one line.

For winter, the initial temperature at the beginning of winter is higher than the mean winter temperature, and thus using T_o only would overestimate $\overline{T}$ (Figure 5a). Similarly, T_o would underestimate $\overline{T}$ for spring. R^2 values of linear regression for spring are higher than that of winter, but the S values are both less than 1, indicating larger year-to-year variability of T_o than that of $\overline{T}$. This is consistent with Figure 4.

Bringing in the ocean advective flux does not significantly change the overall picture. For mean winter temperature, both the R^2 and S are even smaller compared to the case without ocean advection (Figure 5b). For spring, adding ocean advection increases the R^2 and S, suggesting an increased skill in estimating the mean spring temperature (Figure 5d). However, the fact that all data points are located above the one-to-one line means the combination of T_o and $\overline{T_{adv}}$ underestimates the mean spring temperature. In both cases, initial temperature and ocean advection are not sufficient to describe the seasonal mean temperature. Additional cooling (warming) in addition to ocean advection is needed to further describe the winter (spring) temperature.

In comparison, using the sum of the initial temperature and air-sea flux yields a much better description of seasonal mean temperatures (Figures 5c and 5f). The estimates of mean winter temperature based on $T_o + \overline{T_{air}}$ lie around the one-to-one line, with the highest R^2 (=0.78) and S (=0.78) compared to the other two cases for winter. The estimates of mean spring temperature based on $T_o + \overline{T_{air}}$ give an even better result than the corresponding winter estimates. The R^2 value is 0.86 and the S is 0.86. Therefore, to first order, the mean winter/spring temperature can be described by the initial temperature of the season and the mean cumulative air-sea flux reasonably well. We do note the scatter in Figures 5c and 5f, which are primarily due to the missing ocean advection. While the overall role of ocean advection is smaller than that of air-sea flux in determining the winter and spring temperatures, the year-to-year changes in the relative importance is worth investigating.

It was suggested that the air-sea flux played a major role in the development of the extreme warm anomaly in the MAB in winter and spring of 2012 [*Chen et al*., 2014a, 2015]. Because of the large interannual variability of MAB temperature, especially the winter temperature (Figure 3), it is necessary to understand how the relative contributions from the atmosphere and ocean might change from year to year, especially for the extreme years. For comparison purposes, we quantify the relative importance of air-sea and ocean advective fluxes for relative warm and cold years. The categorization of warm/cold years is based on the winter MAB SST. In this case, the MAB SSTs in the winters of 2005 and 2011 are the two coldest, and MAB SSTs in the winters of 2007 and 2012 are the two warmest (Figure 3).

Our focus is on the evolution of temperature anomalies, and we thus remove the mean seasonal cycle of each term (volume-averaged quantities). As such,

$$T_t{}^a = Q_{air}^a + Q_{adv}^a \tag{3}$$

where $T_t = \frac{\partial T}{\partial t}$, $Q_{air} = \frac{Q}{\rho_o c_p H}$, and $Q_{adv} = -\frac{1}{H}\int_{-H}^{0} \nabla(\mathbf{u}T)dz$. Superscript a denotes the daily anomalies with respect to the 12 year mean values of each term. The cumulative form is,

$$dT^a = T_{air}^a + T_{adv}^a \tag{4}$$

where $dT^a = T^a - T_o^a$ is the volume-averaged temperature anomaly change, from time t_1 to time t. To include the information of the temperature anomaly, we add volume-averaged temperature anomaly at the beginning of winter to all three terms in (4) so the initial values of the three terms do not start from zero (Figure 6). Doing so allows us to discuss both the heat flux terms and the temperature anomalies.

In 2005, the temperature anomaly was −0.7°C at the beginning of winter, and it shows strong fluctuations through the winter and spring (Figure 6a). The anomaly ranges from −0.1°C in mid-January to −1.8°C in late January. The fluctuation is controlled by both the cumulative air-sea and ocean advective fluxes. The RMS difference (RMSD) between the temperature anomaly and T_{air}/T_{adv} during winter-spring of 2005 is 1.1/0.76°C, suggesting the ocean advective flux played a more important role in controlling the winter-spring temperature anomalies. In another cold year, 2011, the evolution of the temperature anomaly is relatively more monotonic. The anomaly began as −2.3°C and its magnitude increased toward zero and developed a positive anomaly in early April (Figure 6c). This evolution closely follows T_{air}, and departs from T_{adv}.

In the winter of both 2007 and 2012, the MAB temperature was relatively warm, but the evolutions of the warm anomalies are different. The temperature anomaly in 2007 began as 1.4°C, but decreased through

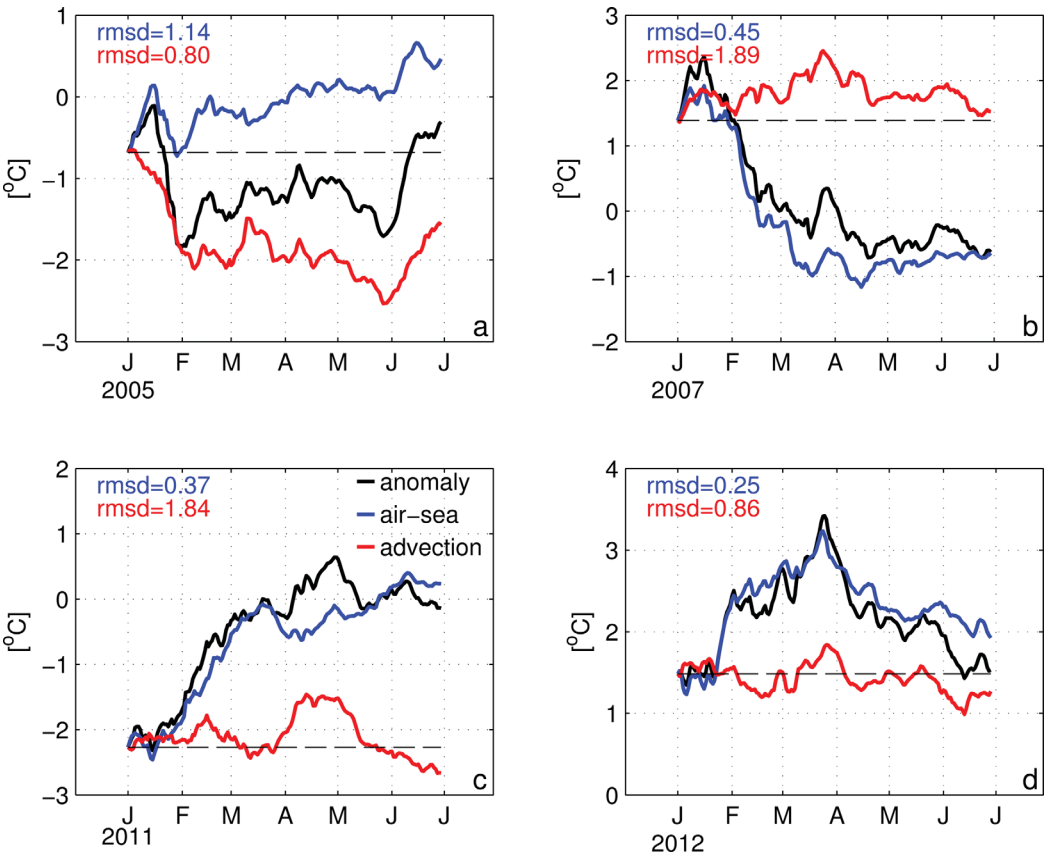

Figure 6. Comparison of the cumulative temperature anomaly budget (based on equation (4)) for relatively warm and cold years. Root-mean-square difference between the temperature anomaly and the cumulative air-sea flux (ocean advective flux) is shown in blue (red).

winter and turned negative in spring. The dramatic change of temperature anomaly is clearly controlled by the air-sea flux (Figure 6b). RMSD between the temperature anomaly and T_{air} is 0.44°C, much smaller than that of T_{adv}. In 2012, the initial temperature anomaly was 1.5°C, and the anomaly went through a dramatic increase and reached a peak value of 3.4°C in late March. After that, the temperature anomaly gradually decreased during April to June 2012. Despite the different temporal pattern when contrasting 2007 and 2012, the evolutions of the temperature anomalies are both predominantly controlled by the cumulative air-sea flux (Figure 6d). Furthermore, it is worth pointing out how remarkable the evolution of temperature anomaly is during the winter and spring of 2012. Normally, given anomalous initial temperature, T_{air} will act to damp the temperature anomaly, as in winter 2007 or 2011, or even 2005 to some extent. However, in winter 2012, the T_{air} continued to increase the temperature anomaly. This again suggests the atmospheric forcing drove the evolution of the temperature anomaly during the winter and spring of 2012.

It is interesting to note that the seasonal mean temperatures can be better described by the initial temperature and air-sea flux, but the relative importance of air-sea flux versus ocean advection in controlling the evolution of temperature anomalies during winter-spring varies from year to year. To evaluate the two processes, we have chosen RMSD as a metric, which measures the distance between the black curve and the blue/red curve (Figure 6). The process with a smaller RMSD plays a more important role. Besides the relative warm/cold years, we have summarized the RMSD values for winter and spring, respectively, in Tables 1 and 2. Out of the 12 years 2003–2014, the air-sea flux normally dominated the temperature anomaly in the MAB during winter. In only 3 years was the wintertime temperature anomaly primarily controlled by ocean advection. Therefore, in a statistical sense, air-sea flux outweighs ocean advection in determining the intraseasonal evolution of winter temperature anomalies in the MAB. For spring, ocean advection has more control on the temperature anomalies than air-sea flux does, although the difference is smaller (Table 2). In both seasons, the relative importance of air-sea flux and ocean advection does not seem to be related to either the initial or seasonal mean thermal condition of the shelf water (fourth and fifth columns of Tables 1 and 2). This result indicates

Table 1. Root-Mean-Square Difference (RMSD) Between the Temperature Anomaly and Cumulative Air-Sea Heat Flux (T_{air})/Ocean Advective Flux (T_{adv}) as Defined in Equation (4)[a]

Year	T_{air} RMSD	T_{adv} RMSD	Initial T Anomaly	Mean T Anomaly
2003	**0.19**	0.31	−0.27	−0.38
2004	**0.35**	1.36	−0.14	−1.12
2005	0.97	**0.52**	−0.68	−1.09
2006	**0.92**	1.78	−0.20	0.66
2007	**0.50**	1.44	1.39	0.98
2008	1.04	**0.31**	−1.05	0.10
2009	**0.40**	0.63	−0.15	−0.49
2010	**0.13**	0.77	−0.15	−0.82
2011	**0.21**	1.38	−2.27	−1.08
2012	**0.17**	0.97	1.48	2.33
2013	**0.30**	0.67	0.57	0.53
2014	0.68	**0.42**	1.47	0.38

[a]For each year, the smaller RMSD value is shown in bold. The volume-averaged, initial temperature anomaly (initial T anomaly) and seasonal mean temperature anomaly (mean T anomaly) are also shown. Units for all values are °C. All numbers are computed for winter period.

the dynamical processes controlling the winter-spring temperature in the MAB are highly variable. It is the relative contributions of the atmospheric and oceanic processes that determine the shelf temperature from year to year.

4. Decorrelation Scales and Predictability of Shelf Temperature

The complex variability of the air-sea flux and ocean advective flux can be further demonstrated in Figure 7. Both the mean air-sea flux and advective flux over winter-spring change dramatically from year to year. The RMS value of the mean air-sea flux during 2003–2014 is 0.25°C per 30 days, and the RMS value of the mean advective flux is 0.16°C per 30 days. The combined effects of the air-sea and advective fluxes largely control the change of the mean temperature anomaly (Figure 7). It is worth pointing out that although the horizontal diffusion instantaneously is negligible, it is not so when considering temporal averaging over 6 months. In some years, it is comparable to the advective flux, and thus the air-sea flux and advective flux do not add up to the T_t^a terms. Nevertheless, relative to the parameterized diffusion term, it is more intuitive to discuss the air-sea flux and ocean advective flux, and their relative contributions to the temperature anomaly.

The statistics regarding the change of temperature anomaly (T_t^a in Figure 7) indicates the overall persistence of the temperature over 6 months and thus have implications for the seasonal predictability of the shelf temperature anomaly. For example, if one winter is anomalously warm, how well can this predict an anomalously warm spring? The springtime temperature anomaly is related to wintertime temperature anomaly, but the relationship is rather weak (Figure 8a). The R^2 is 0.5, and the regression slope is 0.62, indicating weak predictability of using winter temperature anomaly for spring temperature anomaly. We do notice that in some years, the winter temperature anomaly is a good indicator for spring temperature anomaly. For example, both the winter and spring temperature anomaly in 2012 are ∼2.5°C (upper right point in Figure 8a), because the advective and air-sea fluxes are very small in 2012 (Figure 7). This result suggests that besides the interannual change of seasonal mean temperatures, the persistence of the temperature anomaly of winter-spring also varies from year to year. This implies a shift in the temporal statistics from year to year, implying nonstationarity.

While the predictability of spring temperature based on winter temperature is weak, it is anticipated that over shorter lead time, the prediction of spring temperature is feasible. The correlations between spring mean temperature anomaly and temperature anomalies averaged over 15 day windows from January to March increase toward spring months (Figure 8b). While correlations between January temperature anomalies and spring mean anomalies are not significant, temperature anomalies during February and March are significantly correlated with spring temperature anomaly. The correlation coefficients increase from 0.66 in the first half of February to 0.91 in the second half of March. This suggests that estimation of spring temperature anomaly in the MAB based on the thermal condition 2 months before spring is statistically possible.

Table 2. Same as Table 1, but for Spring

Year	T_{air} RMSD	T_{adv} RMSD	Initial T Anomaly	Mean T Anomaly
2003	0.45	**0.36**	−0.23	−0.77
2004	1.02	**0.35**	−0.90	−0.27
2005	**0.26**	0.31	−1.15	−0.99
2006	0.35	**0.20**	0.80	1.08
2007	0.44	**0.18**	0.30	−0.45
2008	0.45	**0.37**	0.27	0.35
2009	0.68	**0.29**	−0.85	−0.54
2010	0.40	**0.26**	−0.19	−0.11
2011	**0.41**	0.52	−0.31	0.17
2012	**0.46**	0.58	3.01	2.07
2013	**0.19**	0.39	−0.56	−0.24
2014	**0.31**	0.34	−0.32	−0.30

We next use the temporal decorrelation scale of temperature anomalies during winter-

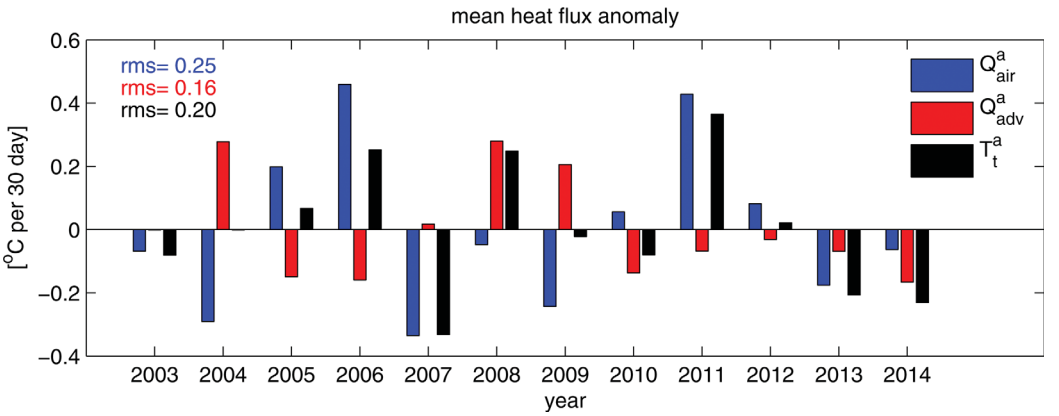

Figure 7. Interannual variability of mean heat flux anomalies (based on equation (3)): mean air-sea flux anomaly (Q^a_{air}), mean ocean advective flux anomaly (Q^a_{adv}), and mean temperature anomaly change (T^a_t) for the winter-spring period. RMS values for each term are shown.

spring to demonstrate the year-to-year changes in the persistence of seasonal mean temperature anomalies (Figure 8c). With the daily climatology removed, the decorrelation scale is defined as the *e*-folding time scale of the volume-averaged temperature anomaly in the MAB. The mean decorrelation scale (*e*-folding scale) for the shelf temperature anomaly in the MAB during winter-spring is ~50 days, which is comparable to the 2 month scale estimated above and shorter than the seasonal scale. This is consistent with the result above that whole winter mean temperature anomaly cannot be used to reliably predict the following spring

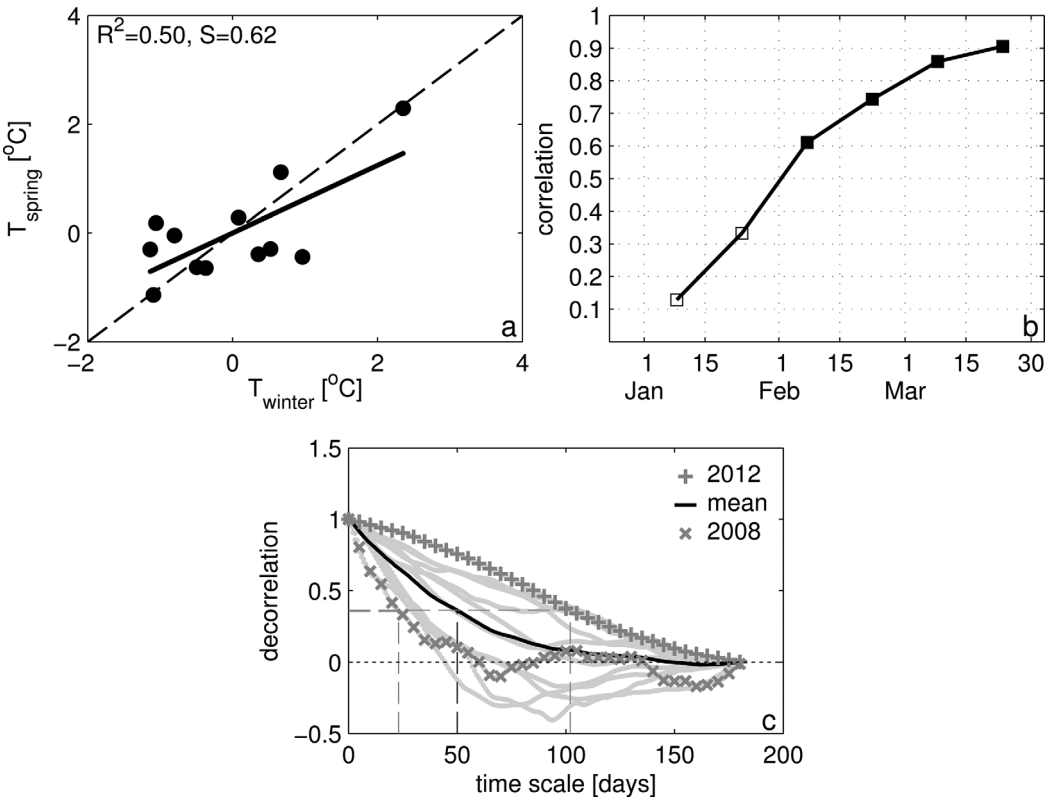

Figure 8. Predictability of winter-spring temperature. (a) Scatterplot for the spring temperature anomaly versus winter temperature anomaly. (b) Correlation between spring mean temperature and temperatures from January to March with a 15 day averaging window. Correlation coefficients significant above (below) 95% confidence level are plotted in closed (open) squares. (c) Temporal decorrelation for the winter-spring period for different years. The solid black line represents the mean from 2003 to 2014.

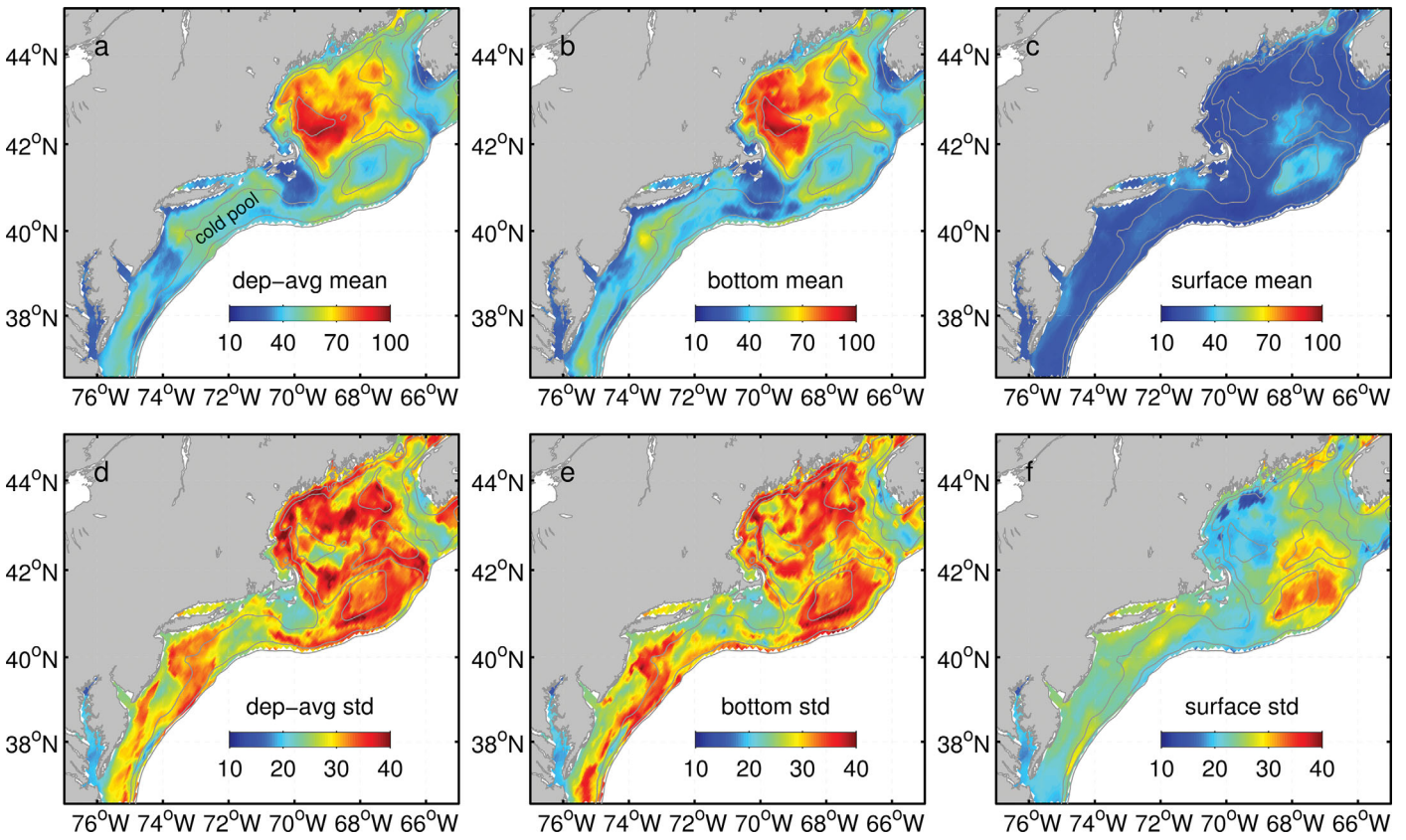

Figure 9. Spatial distribution of the (a–c) 12 year average and (d–f) standard deviation of each winter-spring decorrelation time scale (unit: days) of (a and d) depth-averaged, (b and e) bottom, and (c and f) surface temperatures. The 50, 100, and 200 m isobaths in the model are contoured in gray. The general location of the MAB cold pool is labeled in Figure 9a.

mean temperature anomaly every year. In comparison, the temperature anomaly in 2012 clearly persisted longer into the year. The decorrelation scale in 2012 was ~110 days, more than twice as long as the mean value for 2003–2014. It is consistent with previous analysis that the shelf temperature anomaly started in the fall and winter of 2011–2012 and persisted through spring 2012 [*Chen et al*., 2014a], with potential contributions from an unusual northward shift in the Gulf Stream [*Gawarkiewicz et al*., 2012]. The interannual variability of the decorrelation scale can also be demonstrated by contrasting two extreme years. The decorrelation scale of winter-spring temperature in 2008 has a very short scale of less than 1 month, which indicates the temperature anomaly quickly diminished. The variability of the decorrelation scale largely depends on the relative contributions of air-sea flux and ocean advective flux to the temperature anomaly from year to year. For example, the T_t^a term in 2012 was relatively small compared to that in 2008 as the sum of advective and air-sea fluxes are very small (Figure 7). Correspondingly, the decorrelation scale was also longer in 2012, and shorter in 2008 (Figure 8). We note that T_t^a in Figure 7 is only indicative of the overall decorrelation scale of the temperature anomaly over the whole winter-spring. The decorrelation scale of the shelf temperature anomaly depends on the specific evolution of the temperature anomaly at each instantaneous time, which is determined by the combination of all instantaneous heat flux terms.

Besides the interannual variability of the temporal decorrelation scale of MAB temperature, it is also anticipated that the temporal decorrelation scale varies spatially. We remove the daily climatology of depth-averaged temperature (equivalent to shelf heat content), and present the *e*-folding time scale for temperature anomaly at each grid point in the coastal regions off the Northeast U.S. in Figure 9. In the deep basins of the GoM, the mean decorrelation scale during 2003–2014 is ~70–100 days, longer than that in other regions (Figure 9a). The decorrelation scale at Nantucket Shoals shows a spatial minimum, which is presumably associated with the strong tidal mixing that induced fast heat exchange in and out of the region through both advective flux and air-sea flux [*He and Wilkin*, 2006; *Wilkin*, 2006]. The decorrelation scale is generally shorter at the outer shelf, where complex shelf-slope processes quickly diminish the temperature

anomaly. The decorrelation scale is also relatively longer than surroundings over the central portion of the continental shelf in the Middle Atlantic Bight, roughly in the same location as the Cold Pool [*Houghton et al*., 1982]. The water within the Cold Pool is remnant winter water that is capped by seasonal heating, and the subsurface temperature minimum can persist into fall when the stratification is broken down by convection and wind mixing [*Lentz et al*., 2003]. As a result, the subsurface thermal structure of the cold pool is mixed with the surface layer and the subsurface structure disappears (S. Lentz, personal communication, 2016). The formation and evolution of the MAB cold pool likely explains the longer temporal decorrelation scale of the depth-averaged temperature anomaly over mid-shelf. We note that the decorrelation scale of the mean bottom temperature has a very similar spatial pattern to that of depth-averaged temperature (Figure 9c). For example, both depth-averaged and bottom temperature show the longest decorrelation scale in the GoM, the shortest at Nantucket Shoals, a relatively long scale in the Cold Pool, and a relatively short scale at the shelf break. This indicates the evolution of subsurface thermal structure largely controls the decorrelation scale of the shelf heat content, consistent with the relatively short decorrelation scale of SST (Figure 9e). In addition, the decorrelation scales of shelf heat content and bottom temperature have similar interannual variability (Figures 9b and 9d). The variability is stronger in the GoM, Georges Bank, Hudson Canyon, and the outer shelf. The influence of ocean advection in these regions is subject to considerable interannual variability, and thus is responsible for the changing decorrelation scale from year to year. On the other hand, SST has systematically shorter decorrelation time scales, and shows different spatial distribution of interannual variability (Figures 9e and 9f), compared to both depth-averaged and bottom temperature. This suggests that SST is not appropriate for describing the decorrelation time scale of the shelf heat content in the Northeast U.S. coastal ocean. To better characterize the spatiotemporal variability of the thermal condition of the coastal ocean, we need to rely on numerical modeling and full water column observations rather than satellite SST alone.

5. Discussion

The highly variable air-sea and ocean advective fluxes discussed above directly determine the interannual variability and the seasonal predictability of the shelf temperature in the MAB. Therefore, it is important to understand the primary drivers for the interannual variability of these heat fluxes. *Chen et al*. [2014a] showed that the air-sea heat flux during the extreme event in fall and winter of 2011–2012 is closely associated with the shift of the jet stream latitude over intraseasonal and seasonal time scales. Furthermore, the interannual variability in the jet stream latitude is closely correlated with that of the SST at the NDBC buoy 44008 (Nantucket Shoals) in November–February [*Chen et al*., 2014a]. As the jet stream motion is part of large-scale climate variability, this relationship has important implications on the linkage between continental shelf processes and large-scale atmospheric processes.

We extend the previous analysis focusing on the extreme year of 2012 to other years to examine if the relationship between the air-sea flux and the jet stream latitude is robust for interannual variability across seasons. The air-sea flux within the MAB is calculated as the regional mean within the MAB region (Figure 1). Consistent with previous work [*Bane et al*., 2007; *Barth et al*., 2007; *Chen et al*., 2014a], the latitude of the jet stream is defined as the location of the maximum gradient of geopotential height at 200 hPa along 70°W. Both variables are processed as daily values based on the NCEP NARR product from 1979 to 2014, and their relationship in each season is shown in Figure 10.

Consistent with the analysis of fall and winter of 2011–2012 [*Chen et al*., 2014a], the Pearson correlation between the seasonal mean air-sea flux in the MAB and the seasonal mean latitude of the jet stream are significantly correlated in fall and winter. The correlation coefficient in fall (winter) is 0.37 (0.41), significant at the 95% (95%) confidence level. This suggests that more northly jet stream positions result in larger heat flux from the atmosphere into the ocean in the MAB. This is likely due to warmer and more humid air overlying the continental shelf, which reduces the heat loss from the ocean during the cooling seasons [*Chen et al*., 2014a]. The significant correlation between the jet stream latitude and air-sea flux in fall and winter is also confirmed by comparing the NARR-based jet stream latitude and air-sea flux from OAFlux [*Yu et al*., 2008] (Figure 10, blue lines). The correlation coefficient in fall (winter) is 0.48 (0.36), significant at the 95% (90%) confidence level. In comparison, the correlation in spring and summer breaks down, which indicates the seasonally dependent relationship between the air-sea flux and jet stream latitude. One possible

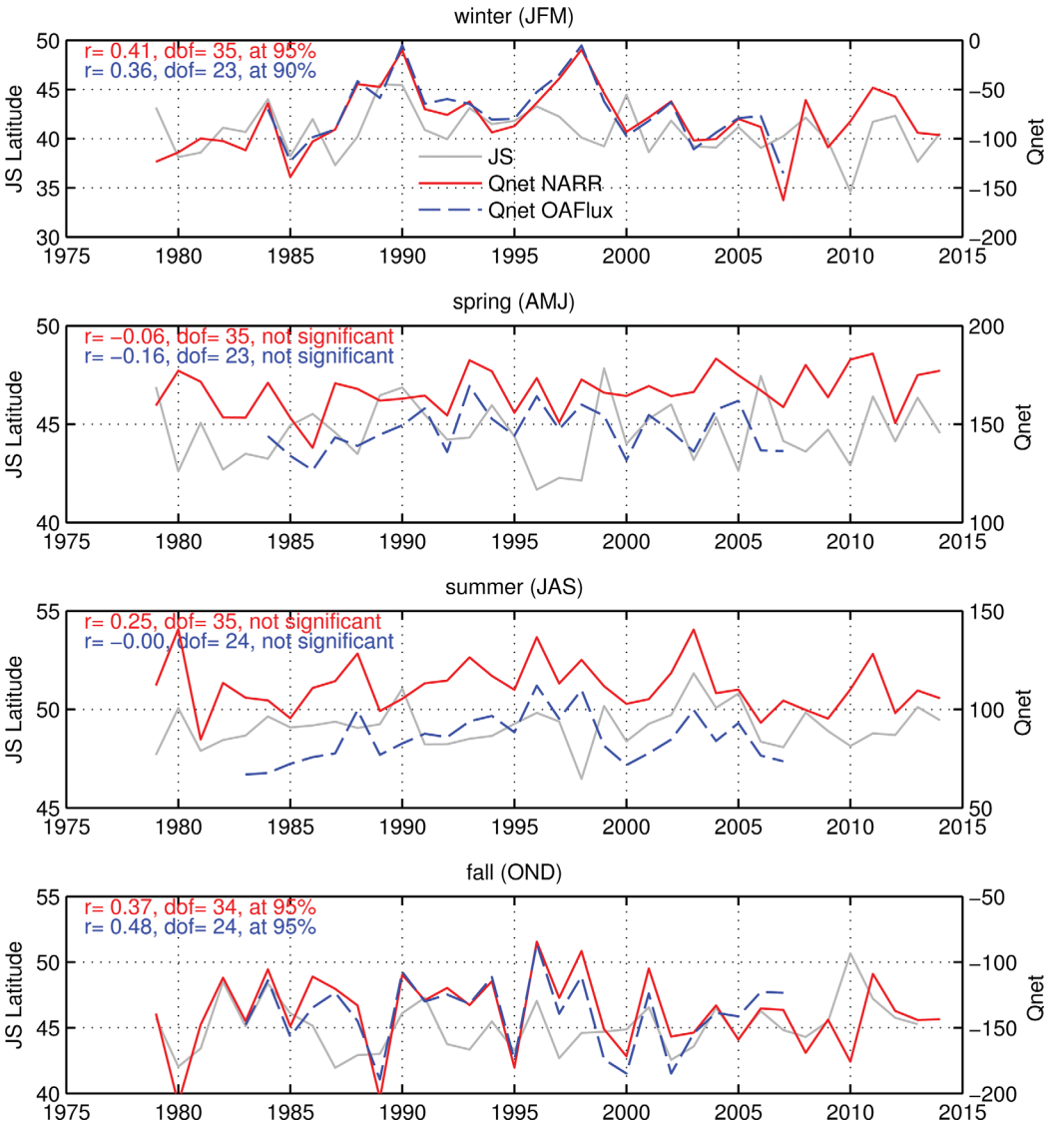

Figure 10. Seasonal mean jet stream latitude (degree north, gray) and air-sea heat flux (W m^{-2}), from NARR (red) and OAFlux (blue), in the MAB. The Pearson correlation coefficients together with the degrees of freedom and significant levels are shown. The correlation is calculated with detrending. Degrees of freedom is calculated based on the integration of autocorrelation considering serial correlation [*Emery and Thomson*, 2001].

explanation is that in spring and summer the mean jet stream latitude is further north, and thus the direct impact of large-scale atmospheric circulation on the MAB region is limited. The other possible explanation is related to the differences in air-sea coupling in different seasons. In fall and winter, because of the deeper mixed layer, the response of SST to air-sea flux is slower than that in spring and summer when the mixed layer is shallower. As a result, air-sea flux, proportional to the air-sea temperature difference, would largely be determined by the air temperature, which is closely related to the large-scale atmospheric circulation. In spring and summer, the air-sea flux may be less correlated with the air temperature due to the shallowness of the surface mixed layer, and thus may be disconnected from large-scale atmospheric circulation, i.e., jet stream variability.

It is important to consider the uncertainties in heat flux products. As shown in Figure 10, the differences in seasonal mean heat flux in the MAB between NARR and OAFlux are small in fall and winter, but the differences are larger in spring and summer, with an approximate difference of 50 W m^{-2}. Examination of two additional reanalysis products CFSR [*Saha et al.*, 2010] and ERA-interim [*Berrisford et al.*, 2011] shows all four products give different seasonal mean values. Despite the different spatial resolutions, seasonal mean heat

flux from NARR, OAFlux, and CFSR are relatively similar. ERA-interim gives much different heat flux values relative to the other three products in all seasons. The uncertainties in heat flux products pose a challenging problem for studying the ocean heat balance and air-sea interactions in the coastal ocean and highlights the need for observation-based high-resolution heat flux products.

The jet stream latitude is also connected to large-scale climate indicators including the Pacific Decadal Oscillation (PDO) index [*Mantua et al*., 1997] and the NINO3.4 index [*Trenberth*, 1997], especially in wintertime. This connection represents an atmospheric pathway from the Pacific to the Atlantic, and has important value in the prediction of seasonal jet stream variability and thus the temperature anomalies in the coastal ocean in the northeastern U.S. Investigation of the mechanistic linkage is beyond the scope of this study, and detailed results on this topic will be reported in the future.

Besides the linkage of the heat content in the coastal ocean to atmospheric large-scale forcing, large-scale oceanic processes also impact the shelf circulation and thus heat content. For example, *Bane et al*. [1988] demonstrated that a shoreward shift in the Gulf Stream position coincides with stronger equatorward flow at the 1000 m isobath in the southern MAB. This suggests that the Gulf Stream may influence the current fluctuations over the upper slope and shelf break by changing the gradient of the sea surface height across the slope gyre [*Csanady and Hamilton*, 1988]. *Fratantoni and Pickart* [2003] performed similar investigations based on a satellite detected Gulf Stream position index and a current meter at the upper continental slope to the south of New England. However, they found no significant correlation between monthly averaged Gulf Stream positions and monthly averaged currents on the upper slope. Furthermore, in each of these studies, there were not sufficient observations to conduct a detailed examination of the impact on the heat budget over the continental shelf or slope. On the other hand, *Rossby and Benway* [2000] and *Peña-Molino and Joyce* [2008] suggested that the change of the Gulf Stream path is a result of thermohaline forcing instead of basin scale wind-driven forcing: shelf and/or slope water transport from the Labrador Sea is able to change the Gulf Stream path. Better understanding of the complex relationship between the Gulf Stream and shelf circulation is an on-going research topic, and also requires further investigation in the future.

Current work focuses on the heat budget and temperature in the MAB during winter and spring. It is worth reiterating that thermal conditions at the beginning of the seasons play an important role in setting the seasonal mean temperatures (Figure 4). In other words, the shelf thermal condition at the end of fall, which is determined by cumulative air-sea flux and ocean advective flux in fall (and even summer), would influence the seasonal mean thermal condition in winter and spring. These connections between seasons indicate the inherent memory of the ocean and highlight the complexity of the interannual variability of shelf temperature. Despite the importance of the initial condition at the beginning of the seasons, it is the flux terms that adjust the initial temperatures and also determines the seasonal mean temperatures. This is particularly true for the MAB, where the mean decorrelation scale of the temperature anomaly in winter and spring is about 50 days accompanied by strong interannual variability.

The mean decorrelation time scale for winter temperature presented in this study (50 days) is shorter than that presented by *Thompson et al*. [1988] (6 months), who used a mixed-layer model to explain the persistence of winter anomalies. The discrepancy could be related to the different spatial and temporal scales of these two studies. *Thompson et al*. [1988] looked at the SST anomaly over a much larger spatial scale including both coastal seas and the open ocean. The 6 month decorrelation scale was derived from the first EOF (Empirical Orthogonal Function) mode, which represents the coherent variability of SST anomaly over the entire Northwest Atlantic. This large-scale variability is most likely caused by the atmospheric forcing via changing the mixed layer depth. Ocean advection is too slow (considering the large region) to erase the anomaly signal over 6 months. However, for smaller spatial variability or a smaller region, e.g., EOF mode 2 in *Thompson et al*. [1988] and this study, the advective flux (together with air-sea flux) can diminish the anomaly signal rather quickly. So the temporal decorrelation scale can be short over the continental shelf. Also, the EOF analysis in *Thompson et al*. [1988] was based on monthly mean SST anomalies. Our calculation is based on daily anomalies during winter-spring, and thus is able to capture a wider spectrum of anomaly variability. The use of daily anomalies allows us to resolve the short-term variability in Figure 8.

The relative importance of atmospheric and oceanic forcing in controlling the shelf temperature changes is highly complex. Over the long-term scale, temperature changes over the entire Northwest U.S. coastal ocean may be controlled by the along-shelf advection [*Shearman and Lentz*, 2010], interannual changes of

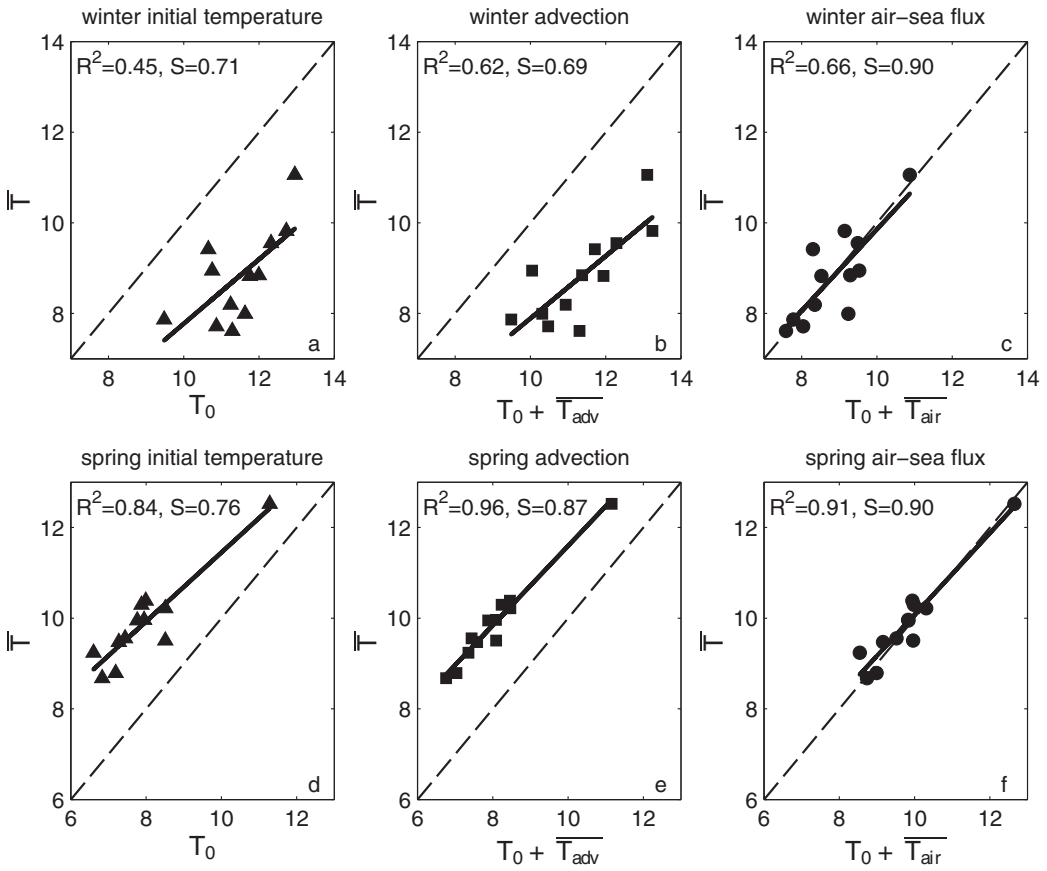

Figure A1. The relationship between winter and spring temperatures and different terms as defined in equation (2). (a and d) Initial temperature, (b and e) initial temperature and mean cumulative ocean advective flux, and (c and f) initial temperature and mean cumulative air-sea flux (unit: °C). R-squared (R^2) and regression slopes (S) are shown. The results are based on numerical simulations with heat flux correction using relaxation coefficients based on the bulk flux formulas [*Barnier et al.*, 1995].

winter and spring temperature in the MAB are predominantly controlled by air-sea flux anomalies. This is largely consistent with the results presented by *Thompson et al.* [1988], although our work focused on the whole water column in the MAB whereas *Thompson et al.* [1988] discussed the SST over the shelf and slope of the entire Northwest Atlantic. Note the temperature discussed here is for the control volume of the MAB, not a specific location in the MAB, where ocean advection could be important in controlling the temperature variability [e.g., *Connolly and Lentz*, 2014; *Forsyth et al.*, 2015]. The implications of studying the temperature variability in the control volume instead of focusing on a certain location or a certain layer (e.g., upper mixed layer or bottom layer) is that impacts of climate variability to the ecosystem such as migration of fish stocks are affected by the thermal condition of the entire water column on the shelf, not SST or temperature at one specific location. Discussing how the advective flux transforms the temperature structure within the control volume is not the focus of the current work, and is something we are interested in exploring in the future.

6. Summary

We investigated the relative contributions of atmospheric and oceanic processes controlling the interannual variability of the shelf temperature in the MAB. A carefully designed regional ocean model is used to complement the limited subsurface observations on the shelf, particularly over long time scales. Built upon previous modeling studies [*Chen et al.*, 2015], the model has sufficient capability to resolve the variability of shelf temperature from year to year. Specifically, the model surface temperature anomalies during winter and spring compare well with buoy temperature anomalies in the same time frame, with a R^2 no less than

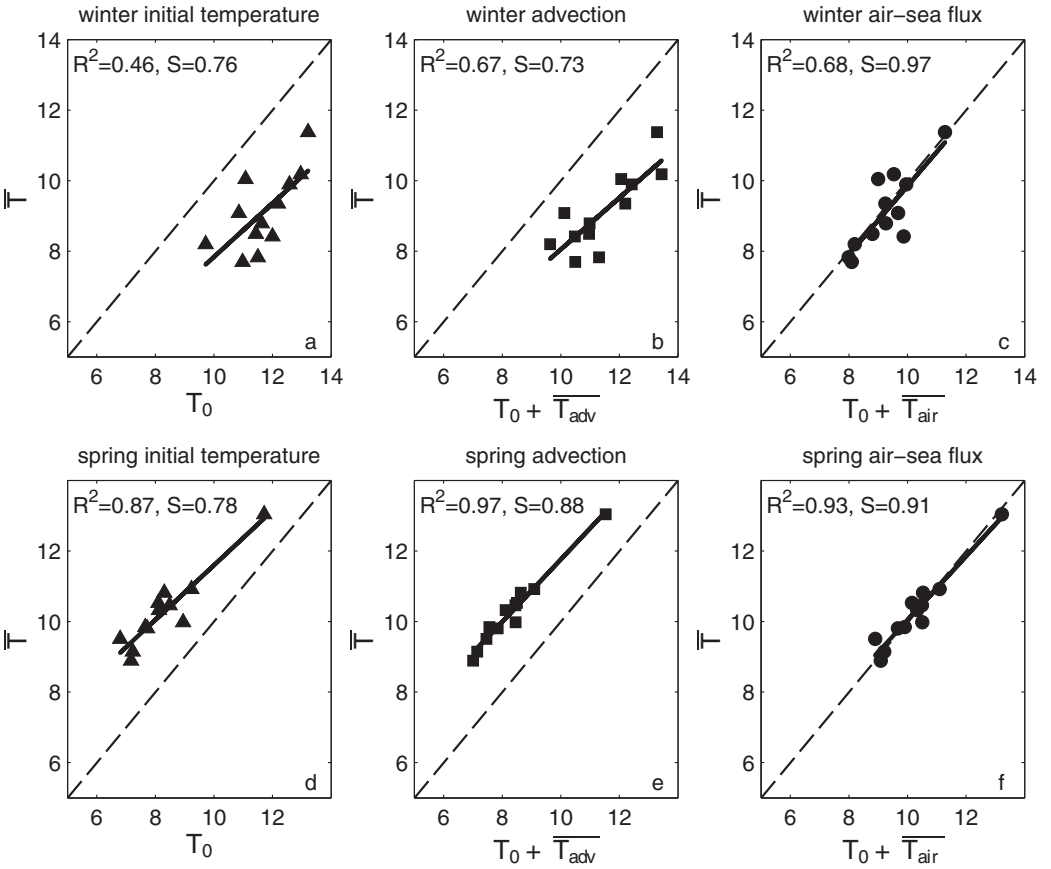

Figure A2. Same as Figure A1, but for the numerical simulations without heat flux correction.

0.8 and a regression slope close to 1. Regional mean SST in the MAB was accurately simulated for both winter and spring from 2003 to 2014.

The mean winter/spring temperature can be described by the combination of the initial temperature at the beginning of the season (T_o), the mean cumulative air-sea flux ($\overline{T_{air}}$), and the mean cumulative ocean advective flux ($\overline{T_{adv}}$). All three terms have large interannual variability, and contribute to the seasonal mean temperature with varying degree from year to year. Over interannual time scales, the mean winter/spring temperature in the MAB can be better described by T_o and $\overline{T_{air}}$. In contrast, using T_o and $\overline{T_{adv}}$ would overestimate (underestimate) mean winter (spring) temperature. In spite of the overall importance of air-sea flux in determining the winter and spring temperature, the dominance between air-sea flux and ocean advective flux on the evolution of the temperature anomaly in each individual year is different. While air-sea flux controls the winter temperature anomalies in the MAB in most years during 2003–2014, ocean advection has more controls on the spring temperature anomalies.

The relative contributions of the atmosphere-ocean heat flux and the oceanic advective flux determine the decorrelation time scale of the temperature anomaly during winter-spring. This has implications on the seasonal predictability of the MAB thermal condition, since the decorrelation time scale may vary by a factor of two from year to year. Overall, winter temperature anomaly is just a moderate indicator of the spring temperature anomaly. This is because of the strong interannual variability of decorrelation time scale, which is controlled by both atmospheric and oceanic processes. Nevertheless, the predictability of spring temperature anomaly within a 2 month time scale is more tractable.

Results from this study identified the complexity of the coastal atmosphere-ocean system accompanied by large interannual variability. These shelf processes control the heat balance in the coastal ocean, and are connected to large-scale circulation, e.g., the jet stream and the Gulf Stream. Better understanding of these local atmospheric and oceanic processes and their linkages to the large-scale processes will provide the

scientific basis necessary for the ecosystem management and thus has important economic impacts for the commercial fishing industry.

Appendix A

In this section, we demonstrate the sensitivity of the results to the flux correction mentioned in section 2.1. Again, the rationale of using the correction scheme was to reduce the uncertainties in heat flux computed based on atmospheric variables from the coarser (than our model) resolution reanalysis. The main results in this work should not depend on this numerical treatment.

To quantify the sensitivity of the results to the strength of heat flux correction, we performed one set of simulations using spatial varying relaxation coefficients based on the bulk flux formulas, calculated based on NARR [*Barnier et al*., 1995], and the other set of simulations without correcting the air-sea heat flux. The results (Figures A1 and A2) are very similar to those using 3 h adjustment scale (Figure 5) in that all major conclusions in section 3 hold. Using T_o only would overestimate (underestimate) $\overline{T}$ in winter (spring), and adding $\overline{T_{adv}}$ does not change the overall picture. In comparison, the combination of T_o and $\overline{T_{air}}$ gives the best estimate of the seasonal mean temperatures.

We have repeated other calculations discussed in the text, and confirm that the choice of correction scheme does not change the major conclusions of this work. Therefore, the approach outlined in section 2 is justified.

Acknowledgments
This work was supported by the National Science Foundation under grant OCE-1435602. K.C. appreciates useful discussions with Steven Lentz and Jiayan Yang. Weifeng (Gordon) Zhang kindly sponsored computation resource at the Scylla/Kenny cluster at WHOI. Constructive comments from two anonymous reviewers are also appreciated. Data used in this work are available upon request at kchen@whoi.edu.

References

Bane, J. M., O. B. Brown, R. H. Evans, and P. Hamilton (1988), Gulf-Stream remote forcing of Shelfbreak Currents in the Mid-Atlantic Bight, *Geophys. Res. Lett.*, *15*(5), 405–407, doi:10.1029/Gl015i005p00405.

Bane, J. M., Y. H. Spitz, R. M. Letelier, and W. T. Peterson (2007), Jet stream intraseasonal oscillations drive dominant ecosystem variations in Oregon's summertime coastal upwelling system, *Proc. Natl. Acad. Sci. U. S. A.*, *104*(33), 13,262–13,267, doi:10.1073/pnas.0700926104.

Barnier, B., L. Siefridt, and P. Marchesiello (1995), Thermal forcing for a global ocean circulation model using a three-year climatology of ECMWF analyses, *J. Mar. Syst.*, *6*(4), 363–380, doi:10.1016/0924-7963(94)00034-9.

Barth, J. A., B. A. Menge, J. Lubchenco, F. Chan, J. M. Bane, A. R. Kirincich, M. A. McManus, K. J. Nielsen, S. D. Pierce, and L. Washburn (2007), Delayed upwelling alters nearshore coastal ocean ecosystems in the northern California current, *Proc. Natl. Acad. Sci. U. S. A.*, *104*(10), 3719–3724.

Berrisford, P., D. Dee, P. Poli, R. Brugge, K. Fielding, M. Fuentes, P. Kallberg, S. Kobayashi, S. Uppala, and A. Simmons (2011), *The ERA-Interim Archive Version 2.0, ERA Rep. Ser.*, vol. 1, ECMWF, Reading, U. K.

Chapman, D. C. (1985), Numerical treatment of cross-shelf open boundaries in a barotropic coastal ocean model, *J. Phys. Oceanogr.*, *15*(8), 1060–1075, doi:10.1175/1520-0485(1985)015<1060:NTOCSO>2.0.CO;2.

Chassignet, E. P., H. E. Hurlburt, O. M. Smedstad, G. R. Halliwell, P. J. Hogan, A. J. Wallcraft, R. Baraille, and R. Bleck (2006), The HYCOM (HYbrid Coordinate Ocean Model) data assimilative system, *J. Mar. Syst.*, *65*(1–4), 60–83.

Chen, K., and R. He (2010), Numerical investigation of the Middle Atlantic Bight shelfbreak frontal circulation using a high-resolution ocean hindcast model, *J. Phys. Oceanogr.*, *40*(5), 949–964, doi:10.1175/2009JPO4262.1.

Chen, K., and R. He (2015), Mean circulation in the coastal ocean off northeastern North America from a regional-scale ocean model, *Ocean Sci.*, *11*(4), 503–517, doi:10.5194/os-11-503-2015.

Chen, K., G. G. Gawarkiewicz, S. J. Lentz, and J. M. Bane (2014a), Diagnosing the warming of the Northeastern U.S. Coastal Ocean in 2012: A linkage between the atmospheric jet stream variability and ocean response, *J. Geophys. Res. Oceans*, *119*, 218–227, doi:10.1002/2013JC009393.

Chen, K., R. He, B. S. Powell, G. G. Gawarkiewicz, A. M. Moore, and H. G. Arango (2014b), Data assimilative modeling investigation of Gulf Stream Warm Core Ring interaction with continental shelf and slope circulation, *J. Geophys. Res. Oceans*, *119*, 5968–5991, doi:10.1002/2014JC009898.

Chen, K., G. Gawarkiewicz, Y.-O. Kwon, and W. G. Zhang (2015), The role of atmospheric forcing versus ocean advection during the extreme warming of the Northeast U.S. continental shelf in 2012, *J. Geophys. Res. Oceans*, *120*, 4324–4339, doi:10.1002/2014JC010547.

Connolly, T. P., and S. J. Lentz (2014), Interannual variability of wintertime temperature on the inner continental shelf of the Middle Atlantic Bight, *J. Geophys. Res. Oceans*, *119*, 6269–6285, doi:10.1002/2014JC010153.

Coumou, D., and S. Rahmstorf (2012), A decade of weather extremes, *Nat. Clim. Change*, *2*(7), 491–496.

Csanady, G. T., and P. Hamilton (1988), Circulaton of the slope water, *Cont. Shelf Res.*, *8*(5–7), 565–624.

Emery, W. J., and R. E. Thomson (2001), Statistical methods and error handling, in *Data Analysis Methods in Physical Oceanography*, edited by W. J. E. E. Thomson, chap. 3, pp. 193–304, Elsevier Sci., Amsterdam, doi:10.1016/B978-044450756-3/50004-6.

Fairall, C. W., E. F. Bradley, J. E. Hare, A. A. Grachev, and J. B. Edson (2003), Bulk parameterization of air–sea fluxes: Updates and verification for the COARE algorithm, *J. Clim.*, *16*(4), 571–591, doi:10.1175/1520-0442(2003)016<0571:BPOASF>2.0.CO;2.

Forsyth, J. S. T., M. Andres, and G. G. Gawarkiewicz (2015), Recent accelerated warming of the continental shelf off New Jersey: Observations from the CMVOleander expendable bathythermograph line, *J. Geophys. Res. Oceans*, *120*, 2370–2384, doi:10.1002/2014JC010516.

Fratantoni, P. S., and R. S. Pickart (2003), Variability of the shelfbreak jet in the Middle Atlantic Bight: Internally or externally forced?, *J. Geophys. Res.*, *108*(C5), 3166, doi:10.1029/2002JC001326.

Friedland, K. (2012), Ecosystem advisory for the Northeast Shelf Large Marine Ecosystem, Advisory 2012, *Rep. 2*, Northeast Fishery Science Center, Woods Hole, Mass.

Gawarkiewicz, G. G., R. E. Todd, A. J. Plueddemann, M. Andres, and J. P. Manning (2012), Direct interaction between the Gulf Stream and the shelfbreak south of New England, *Sci. Rep.*, *2*, 553, doi:10.1038/srep00553, Woods Hole, Mass.

Gawarkiewicz, G. G., G. Lawson, M. Petruny-Parker, P. Fratantoni, and J. Hare (2013), The shelf break ecosystem off the northeastern United States: Current issues and recommended research directions, report, 29 pp., Coop. Inst. for the North Atl. Reg.
Haidvogel, D. B., et al. (2008), Ocean forecasting in terrain-following coordinates: Formulation and skill assessment of the Regional Ocean Modeling System, *J. Comput. Phys.*, *227*(7), 3595–3624, doi:10.1016/j.jcp.2007.06.016.
Hansen, J., M. Sato, and R. Ruedy (2012), Perception of climate change, *Proc. Natl. Acad. Sci. U. S. A.*, *109*, E2415–23, doi:10.1073/pnas.1205276109.
He, R., and J. L. Wilkin (2006), Barotropic tides on the southeast New England shelf: A view from a hybrid data assimilative modeling approach, *J. Geophys. Res.*, *111*, C08002, doi:10.1029/2005JC003254.
Houghton, R. W., R. Schlitz, R. C. Beardsley, B. Butman, and J. L. Chamberlin (1982), The Middle Atlantic Bight Cold Pool: Evolution of the temperature structure during summer 1979, *J. Phys. Oceanogr.*, *12*(10), 1019–1029, doi:10.1175/1520-0485(1982)012<1019:TMABCP>2.0.CO;2.
Joyce, T. M. (2002), One hundred plus years of wintertime climate variability in the eastern United States, *J. Clim.*, *15*(9), 1076–1086, doi:10.1175/1520-0442(2002)015<1076:OHPYOW>2.0.CO;2.
Ketchum, B. H., and N. Corwin (1964), The persistence of "winter" water on the continental shelf of Long Island, New York, *Limnol. Oceanogr., IX*(4), 467–475.
Lentz, S., K. Shearman, S. Anderson, A. Plueddemann, and J. Edson (2003), Evolution of stratification over the New England shelf during the Coastal Mixing and Optics study, August 1996–June 1997, *J. Geophys. Res.*, *108*(C1), 3008, doi:10.1029/2001JC001121.
Lentz, S. J. (2010), The mean along-isobath heat and salt balances over the middle Atlantic bight continental shelf, *J. Phys. Oceanogr.*, *40*(5), 934–948, doi:10.1175/2009JPO4214.1.
Lucey, S. M., and J. A. Nye (2010), Shifting species assemblages in the Northeast US Continental Shelf Large Marine Ecosystem, *Mar. Ecol. Prog. Ser.*, *415*, 23–33, doi:10.3354/meps08743.
Luettich, R. A., J. J. Westerink, and N. W. Scheffner (1992), ADCIRC: An advanced three-dimensional circulation model for shelves, coast, and estuaries, Report 1. Theory and methodology of ADCIRC-2DDI and ADCIRC-3DL, *Tech. Rep. DPR-92-6*, 137 pp., U.S. Army Corps of Eng., Vicksburg, Miss.
Mantua, N. J., S. R. Hare, Y. Zhang, J. M. Wallace, and R. C. Francis (1997), A Pacific Interdecadal Climate Oscillation with Impacts on Salmon Production, *Bull. Am. Meteorol. Soc.*, *78*(6), 1069–1079, doi:10.1175/1520-0477(1997)078<1069:APICOW>2.0.CO;2.
Mason, E., J. Molemaker, A. F. Shchepetkin, F. Colas, J. C. McWilliams, and P. Sangrà (2010), Procedures for offline grid nesting in regional ocean models, *Ocean Model.*, *35*(1–2), 1–15, doi:10.1016/j.ocemod.2010.05.007.
Miller, C. B. (2004), *Biological Oceanography*, 416 pp., Wiley-Blackwell, Malden, Mass.
Mills, K., et al. (2013), Fisheries management in a changing climate: Lessons from the 2012 ocean heat wave in the Northwest Atlantic, *Oceanography*, *26*, 191–195.
Mountain, D. G. (2003), Variability in the properties of Shelf Water in the Middle Atlantic Bight, 1977–1999, *J. Geophys. Res.*, *108*(C1), 3014, doi:10.1029/2001JC001044.
Nye, J. A., J. S. Link, J. A. Hare, and W. J. Overholtz (2009), Changing spatial distribution of fish stocks in relation to climate and population size on the Northeast United States continental shelf, *Mar. Ecol. Prog. Ser.*, *393*, 111–129, doi:10.3354/meps08220.
Orlanski, I. (1976), A simple boundary condition for unbounded hyperbolic flows, *J. Comput. Phys.*, *21*(3), 251–269.
Peña-Molino, B., and T. M. Joyce (2008), Variability in the slope water and its relation to the Gulf Stream path, *Geophys. Res. Lett.*, *35*, L03606, doi:10.1029/2007GL032183.
Rahmstorf, S., and D. Coumou (2011), Increase of extreme events in a warming world, *Proc. Natl. Acad. Sci. U. S. A.*, *108*, 17,905–17,909, doi:10.1073/pnas.1101766108.
Rossby, T., and R. L. Benway (2000), Slow variations in mean path of the Gulf Stream east of Cape Hatteras, *Geophys. Res. Lett.*, *27*(1), 117–120, doi:10.1029/1999GL002356.
Saha, S., et al. (2010), The NCEP climate forecast system reanalysis, *Bull. Am. Meteorol. Soc.*, *91*(8), 1015–1057, doi:10.1175/2010BAMS3001.1.
Shchepetkin, A. F., and J. C. McWilliams (2005), The regional oceanic modeling system (ROMS): A split-explicit, free-surface, topography-following-coordinate oceanic model, *Ocean Model.*, *9*(4), 347–404, doi:10.1016/j.ocemod.2004.08.002.
Shearman, R. K., and S. J. Lentz (2010), Long-term sea surface temperature variability along the U.S. east coast, *J. Phys. Oceanogr.*, *40*, 1004–1016.
Thompson, K. R., R. H. Loucks, and R. W. Trites (1988), Sea surface temperature variability in the shelf-slope region of the Northwest Atlantic, *Atmos. Ocean*, *26*(2), 282–299.
Todd, R. E., G. G. Gawarkiewicz, and W. B. Owens (2012), Horizontal scales of variability over the Middle Atlantic Bight shelf break and continental rise from finescale observations, *J. Phys. Oceanogr.*, *43*(1), 222–230, doi:10.1175/JPO-D-12-099.1.
Trenberth, K. E. (1997), The Definition of El Niño, *Bull. Am. Meteorol. Soc.*, *78*(12), 2771–2777, doi:10.1175/1520-0477(1997)078<2771:TDOENO>2.0.CO;2.
Walsh, H. J., D. E. Richardson, K. E. Marancik, and J. A. Hare (2015), Long-term changes in the distributions of larval and adult fish in the Northeast U.S. shelf ecosystem, *PLoS ONE*, *10*(9), e0137382, doi:10.1371/journal.pone.0137382.
Warner, J. C., C. R. Sherwood, H. G. Arango, and R. P. Signell (2005), Performance of four turbulence closure models implemented using a generic length scale method, *Ocean Model.*, *8*(1–2), 81–113, doi:10.1016/j.ocemod.2003.12.003.
Wilkin, J. L. (2006), The summertime heat budget and circulation of southeast new England shelf waters, *J. Phys. Oceanogr.*, *36*(11), 1997–2011, doi:10.1175/JPO2968.1.
Yu, L., X. Jin, and R. A. Weller (2008), Multidecade global flux datasets from the Objectively Analyzed Air-sea Fluxes (OAFlux) project: Latent and sensible heat fluxes, ocean evaporation, and related surface meteorological variables, report, ref no. OA-2008-01, 64 pp., Woods Hole, Mass.